EUROPEAN
JOURNAL OF
MECHANICS
B/FLUIDS

# Scale analysis and experimental observations of shock-induced turbulent boundary layer separation in nozzles

Russell G. Keanini [a,*], Andrew M. Brown [b,1]

[a] *The University of North Carolina at Charlotte, Charlotte, NC 28223-0001, USA*
[b] *NASA Marshall Space Flight Center, Huntsville, AL, USA*

## Abstract

Time average shock-induced boundary layer separation is investigated using scale analyses, analytical modeling, and experiments. While the study focuses on turbulent boundary layer separation in overexpanded rocket nozzles, many of the analyses presented apply to the broad family of free interaction, shock-separated flows in which the structure of the boundary layer–shock interaction zone is self-similar and independent of the shock generator. The scale analyses lead to two approximate expressions for the wall pressure ratio at separation; over a range of separation Mach numbers, both models provide reasonable predictions of observed separation pressure ratios. The second model, representing a refinement of the first, appears to provide a fairly general description of free interaction separation: the model approximately captures separation pressure ratios observed in supersonic flow over backward facing steps and in the case of overexpanded nozzle flow, provides predictions that are consistent with the free interaction model. Experiments are carried out in a sub-scale nozzle under overexpanded, cold-flow conditions. The principal observations are as follows: (i) For the range of separation Mach numbers investigated ($5.0 \leqslant M_i \leqslant 5.4$), nominal separation line locations can be predicted with reasonable accuracy using the classical generalized quasi-one-dimensional compressible flow model and an appropriate separation criterion. (ii) Over the same range of overexpanded flow conditions, the time-average pressure rise over the shock interaction zone can be accurately fit by the free interaction model.
© 2006 Elsevier Masson SAS. All rights reserved.

*Keywords:* Shock-induced separation; Compressible turbulent boundary layers

## 1. Introduction

Shock-induced separation of turbulent boundary layers represents a long-studied problem in compressible flow, bearing, for example, on applications in high speed aerodynamics, rocketry, wind tunnel design, and turbomachinery. Experimental investigations have generally sought to expose essential physics using geometrically simple configurations, e.g., supersonic flow over compression ramps [1–4], curved surfaces [2], backward and forward facing steps [2], simplified wing shapes [5], and various blunt objects [4,6,7]. While a variety of computational and analytical meth-

---

\* Corresponding author. Department of Mechanical Engineering & Engineering Science. Tel.: +704 687 4158; fax: +704 687 6069.
   *E-mail address:* rkeanini@uncc.edu (R.G. Keanini).
[1] Staff Scientist, Structural Dynamics and Loads Group.

ods have also been developed for treating the problem, the methods are typically applicable to specific compressible flow regimes, i.e., transonic, supersonic or hypersonic flow, and moreover, due to the intrinsic unsteadiness of the separation process, require problem-specific tuning [8,9].

A large class of shock separated turbulent boundary layer flows, including those in overexpanded rocket nozzles [8], exhibit self-similar structure in the vicinity of the nominal (time-average) separation line. Here, the time-average pressure distribution over the shock interaction zone varies in a qualitatively distinct fashion, independent of the downstream obstacle causing the separation-inducing shock [2,10,11]. Similar structure is likewise observed when separation is produced by incident shocks [2]. Since this feature arises in both laminar and turbulent boundary layers, where downstream influence propagates well upstream in laminar boundary layers [12], the self-similar structure of the boundary layer-shock interaction zone reflects co-dominance of the hyperbolic inviscid outer flow and the local compression-induced pressure rise produced by rapid boundary layer thickening [12].

Chapman et al. [2] used these notions to develop the free interaction model of shock-induced separation. The model assumed that local boundary layer thickening and associated compression of the outer flow were coupled and independent of downstream conditions (see Section 3.1 below). Erdos and Pallone [13] formalized Chapman's approach by developing a wall pressure correlation to describe the pressure variation over the boundary layer–shock interaction zone. Carriere et al. [14], focusing on separation in rocket nozzles, extended this approach to include separating flows subject to external pressure gradients, leading to the generalized free interaction model.

This paper investigates time-average, shock-induced turbulent boundary layer separation in over-expanded rocket nozzles. Although focused on this particular problem, much of the development applies to the same broad family of shock-separated flows encompassed by the free interaction model. The objectives are to first present and examine an alternative to the free interaction model, with a view toward obtaining a fuller understanding of the free interaction process. Simple scale analyses of transverse momentum transport across the separating boundary layer are presented and used to derive criteria for estimating the approximate time-average separation pressure ratio, $P_i/P_p$, as a function of the inviscid separation Mach number, $M_i = M(x_i)$, where $P_i$ is the time-average wall pressure at the point of incipient separation, $x_i$, and $P_p$ is the peak wall pressure at the downstream limit of the shock interaction zone, $x_p$; see Fig. 1. In the case of rocket nozzle flows, where separation-induced side loading constitutes an intrinsic feature of low altitude flight [15,16], knowledge of the separation criterion

$$\frac{P_i}{P_p} = F_o(M_i) \tag{1}$$

is crucial since it allows determination of the corresponding separation line location.

Second, we examine the applicability of the free interaction model to shock-separated flow in nozzles. Observations of boundary layer separation in overexpanded rocket nozzles [8,14] indicate that the structure of the time-average shock interaction zone, as revealed by wall pressure measurements, is well-described by the free interaction model. However, since the model incorporates up to four free parameters (as described in Section 3.1 below), the degree to which the model captures the actual physics of separation remains unclear. Focusing on separation pressure ratios predicted by the model, we obtain further evidence of the model's applicability to separating nozzle flows.

Third, the paper experimentally investigates separation in overexpanded rocket nozzles under conditions where the separation Mach number, $M_i$, lies outside the range of validity of the above scale analyses ($M_i \gtrsim 4.5$). Here, for simplicity, observed mean wall pressure variations are studied using the generalized quasi-one-dimensional flow model and a method incorporating the model is presented for predicting the nominal boundary layer separation location as a function of the nozzle pressure ratio (i.e., the ratio of nozzle chamber pressure to ambient pressure). In addition, preliminary results in which the free interaction model is fit to observed time-average shock interaction zone pressure variations are presented.

## 2. Scale analysis of turbulent boundary layer separation

### 2.1. Background

Due to the importance of shock-induced separation in overexpanded rocket nozzles, the problem has received significant attention in the rocket design community [15–21]. This work has been motivated primarily by a desire

to improve nozzle performance under overexpanded flow conditions, generally extant during low altitude, high ambient pressure flight, and to mitigate against nozzle side loads produced by asymmetric boundary layer separation [15,16,22]. Two distinct separation processes have been identified in overexpanded rocket nozzles, free shock separation [8,23], in which the turbulent boundary layer separates without reattachment, and restricted shock separation [16,22], in which the separated boundary layer reattaches, forming a small, closed recirculation zone immediately downstream of the separation point. This article will focus on free shock separation.

The time-average flow features associated with free shock separation in nozzles were first characterized by Summerfield et al. [23], and are depicted schematically in Figs. 1 and 2. As shown, the time average pressure along the nozzle wall increases from $P_i$ at the incipient separation point, $x_i$, to a peak value of $P_p$ at $x_p$. Depending on the nozzle and the shock location relative to the nozzle exit, $P_p$ is typically on the order of 80 to 100% of the ambient pressure, $P_a$. The time-average separation point, $x_s$, lies immediately upstream of $x_p$.
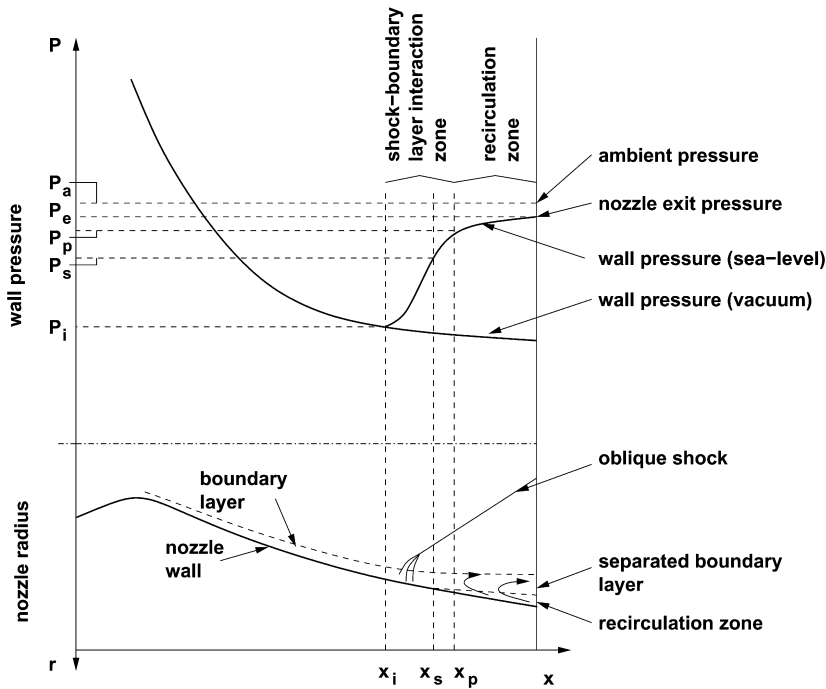


Fig. 1. Schematic of shock-induced boundary layer separation in rocket nozzles. The pressure variation shown is characteristic of free interaction separation problems. Adapted from Ostlund [8].
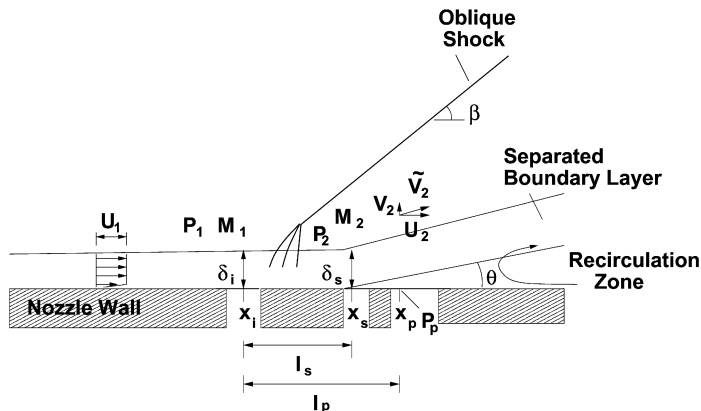


Fig. 2. Detailed view of the boundary layer separation region.

Of central importance in nozzle design is determining both the conditions under which separation will occur and the approximate separation location. A number of criteria, as represented by Eq. (1), have been proposed for predicting the nominal free shock separation point, $x_s$ [8,19,23–28]. These can be grouped into one of three categories: purely empirical correlations having no apparent physical basis [23,25,26], semi-empirical correlations in which a theoretical model is developed and then fitted to data using one or more adjustable parameters [14,19,28], and purely empirical correlations which have an *apparent* though untested physical basis [8,27]. Since the boundary layer pressure rise between $x_i$ and $x_s$ depends primarily on the inviscid flow Mach number, $M_i$ [2,29], most criteria relate either a gross separation pressure ratio, $P_i/P_a$, or more recently, a refined ratio, $P_i/P_p$, to $M_i$ [8]. Given the separation pressure ratio, the separation location can then be determined using an appropriate model of flow upstream of separation.

The last group of criteria above are relevant to the present study. In particular, all criteria in this group are based on the ad hoc assumption that the separation pressure ratio corresponds to the pressure jump across the separation-inducing oblique shock. For turbulent boundary layers, this appears to be a reasonable assumption; Liep-mann et al. [12] demonstrated that rapid thickening of the boundary layer near separation causes associated inviscid compression waves above the boundary layer to rapidly coalesce into an oblique shock. However, there has been no attempt to place this key assumption on a sound physical basis. This section of the paper will attempt to do this.

Although the actual separation process is highly dynamic, in the following we will focus on time average flow dynamics in the vicinity of the shock interaction zone. In order to provide proper physical context, we briefly review the dynamical features associated with free shock separation and note simplifying assumptions to be made. Shock motion over the shock interaction zone appears to be comprised of essentially two components: (i) a low frequency, large scale motion produced by flow variations downstream of the separation point, and occurring over the length of the shock interaction zone, $l_p = x_p - x_i$, at characteristic frequencies, $f_s$ [on the order of 300 to 2000 Hz in the case of compression ramp and backward facing step flows [3,8]], and (ii) a high frequency, low amplitude jitter produced by advection of vortical structures through the shock interaction zone [3]. We will limit attention to time scales that are long relative to $f_s^{-1}$. In addition, it will be assumed throughout that the flow is statistically stationary and that the separation process is two-dimensional. In reality, three-dimensional effects are generally important [8].

The time average pressure gradient over the shock interaction zone ($x_i \leqslant x \leqslant x_p$), given approximately by

$$\frac{\partial P}{\partial x} \sim \frac{P_p - P_i}{l_p} \tag{2}$$

in reality reflects the intermittent, random motion of the shock between $x_i$ and $x_p$ [3]. As the shock-compression wave system oscillates randomly above (and partially within) the boundary layer, the associated pressure jump across the system is transmitted across the boundary layer on a time scale $\tau_s \sim \delta_i/\sqrt{kRT_i}$, where $\delta_i$ and $T_i$ are the characteristic boundary layer thickness and temperature in the vicinity of $x_i$. Under typical experimental conditions, $\tau_s$ is much shorter than the slow time scale, $f_s^{-1}$ (where $\tau_s \approx 1$ to 10 µs); thus, the instantaneous separation point essentially tracks the random position of the shock-compression wave system, where the position of the separation point is described by a Gaussian distribution over the length of the interaction zone [3].

## 2.2. Scale analysis I

Considering the vertical momentum balance immediately downstream of the separation point $x_s$, it is recognized that the boundary layer lifts off of the wall due to a vertical gradient in pressure [2,30]. Thus, the vertical advection of vertical momentum must be of the order of the vertical pressure gradient:

$$\rho v \frac{\partial v}{\partial y} \sim \frac{\partial P}{\partial y} \tag{3}$$

or in approximate form,

$$\rho_2 \frac{v_s^2}{\delta_s} \sim \frac{P_p - P_2}{\delta_s}, \tag{4}$$

where the density $\rho_2$ of the boundary layer near $x_s$ is approximated as the free stream density downstream of the shock, $v_s$ is the characteristic vertical velocity component within the boundary layer near $x_s$, and $\delta_s \approx \delta_i$ is the characteristic boundary layer thickness near $x_s$. Refer to Figs. 1 and 2. The pressure difference across the separating boundary layer,

$P_p - P_2$, is estimated as the difference between the peak wall pressure, $P_p$, in the vicinity of $x_p$ and the free stream pressure immediately downstream of the oblique shock. The density estimate in (4) recognizes that the boundary layer has passed through the compression wave system at the foot of the oblique shock.

Eliminating $\delta_s$ from (4) and solving for $v_s$ yields

$$v_s \sim \sqrt{\frac{P_p - P_2}{\rho_2}}. \tag{5}$$

From Fig. 2, we note that at the separation point, $v_s$ is related to the characteristic horizontal velocity component, $u_s$ by

$$\frac{v_s}{u_s} \sim \tan\theta, \tag{6}$$

where $\theta$ is the characteristic angle of deflection between the separating boundary layer and the nozzle wall. The magnitude of $u_s$ is estimated by again noting that the boundary layer flow has passed through the compression wave system at the foot of the oblique shock and that, as indicated in Fig. 2, the time average turbulent boundary layer velocity profile is nearly flat. Thus, $u_s$ is on the order of the $x$-component ($U_2$) of the inviscid flow velocity ($\tilde{V}_2$) immediately downstream of the oblique shock:

$$u_s \sim U_2 \sim \tilde{V}_2 \cos\theta. \tag{7}$$

Using the ideal gas relation, $\rho_2 = k P_2/(k R T_2)$, and inserting (5) in (6) we then obtain

$$\tan\theta \sim \sqrt{\frac{P_p - P_2}{k P_2}} \frac{1}{M_{2x}}, \tag{8}$$

where $M_{2x} = M_2 \cos\theta$, and $M_2$ is the inviscid flow Mach number immediately downstream of the oblique shock. Rewriting $P_p/P_2$ as $(P_p/P_1)(P_1/P_2)$ and solving (8) for $P_p/P_1$ finally yields

$$\frac{P_1}{P_p} \sim \left[\frac{1}{1 + kM_2^2 \sin^2\theta}\right] \frac{P_1}{P_2}. \tag{9}$$

Identifying $P_1/P_p$ as the critical wall pressure ratio at which separation occurs, i.e., $P_1/P_p \approx P_i/P_p$, noting that $M_2$ is given by the oblique shock relation

$$M_2^2 = \frac{(k+1)M_1^2 \sin^2\beta + 2}{2kM_1^2 \sin^2\beta - (k-1)} \sin^{-2}(\beta - \theta) \tag{10}$$

and recognizing that $M_i \approx M_1$, where $M_1$ is the free stream Mach number immediately upstream of the oblique shock, it is seen that (9) provides an explicit, physically-based relationship between $P_i/P_p$ and the pressure ratio, $P_1/P_2$, across the oblique shock. The next scale analysis refines the estimates for streamwise inertia and cross-layer pressure gradient, and leads to a near-identity between $P_i/P_p$ and $P_1/P_2$.

## 2.3. Scale analysis II

In order to refine the first scaling argument, we base the second analysis on momentum transfer in a curvilinear streamline coordinate system. Thus, in the vicinity of the separation point, $x_s$, and in analogy with the first analysis, we recognize that a fluid particle's normal acceleration component within the separating boundary layer is determined by the normal component of the pressure gradient across the separating boundary layer. Thus, balancing these terms yields:

$$\rho \frac{V_s^2}{R} \sim \frac{\partial P}{\partial n}, \tag{11}$$

where $V_s$ is the particle speed in the streamwise ($s$-) direction, and $R^{-1}$ is the local streamline curvature. The curvature can be evaluated by first defining the shape of the boundary layer's outer-most streamline (i.e., a streamline in the vicinity of $\delta_{99}$ which is roughly parallel to the local displacement thickness) as $r(x) = f(x)$, where $r(x)$ is the radial

distance from the nozzle centerline to the streamline, evaluated at axial position $x$. Thus, $R^{-1} = f''(\sqrt{1 + (f')^2})^{-3}$. Expressing $V_s^2$ in terms of local Cartesian velocity components, $V_s^2 = u_s^2 + v_s^2$, and estimating $u_s$ and $v_s$ by their approximate free stream magnitudes downstream of the oblique shock (since again, at axial position $x_s$, the boundary layer has passed through the compression system below the shock), we obtain $V_s^2 \approx U_2^2 + V_2^2$. Replacing terms in (11) by their approximate magnitudes then leads to

$$\rho_2 \frac{U_2^2 + V_2^2}{R} \sim \frac{P_p - P_2}{\delta_s}, \tag{12}$$

where arguments similar to those used above lead to the given pressure gradient and density estimates.

### 2.3.1. Boundary layer thickness

In order to proceed, we must estimate the magnitude of the boundary layer thickness, $\delta_s$, immediately upstream of the separation point, $x_s$. First, note that at the wall between $x_i$ and $x_s$, the $x$-momentum equation yields the approximate balance

$$\mu \frac{\partial^2 u}{\partial y^2} \sim \frac{\partial P}{\partial x}, \tag{13}$$

where $\mu$ is the dynamic viscosity. Estimating the magnitude of each term in this equation leads to

$$\frac{U_2}{\delta_s^2} \sim \frac{1}{\mu} \frac{P_p - P_1}{l_s}, \tag{14}$$

where, since we are focusing on the neighborhood of $x_s$, $u$ is approximated as $U_2$, and where it is recognized that the streamwise pressure increases from approximately $P_1$ near $x_i$ to approximately $P_p$ near $x_s$. [Although $P$ equals $P_s$ at $x_s$, due to the relatively small difference between $P_s$ and $P_p$, for simplicity, we approximate $P(x_s)$ as $P_p$.] The $x$-length scale, $l_s = (x_s - x_i)$, is approximately equal to the length of the shock interaction zone, $l_p = x_p - x_i$.

Considering the continuity equation near $x_s$, we recognize that since the boundary layer acquires a vertical velocity component as it travels toward and past $x_s$, and since associated mass advection and volumetric dilatation terms, $\rho^{-1}\mathbf{u} \cdot \nabla \rho$, and $\nabla \cdot \mathbf{u}$, respectively, are of the same order, then

$$\frac{\partial u}{\partial x} \approx \frac{\partial v}{\partial y} \tag{15}$$

or in terms of orders of magnitude,

$$\frac{U_2}{l_s} \sim \frac{V_s}{\delta_s}, \tag{16}$$

where again the vertical velocity near $x_s$ is on the order of $V_2$, the inviscid flow's vertical velocity component immediately downstream of the oblique shock. Thus, since $V_2/U_2 \sim \tan \theta$, we obtain the following estimate for $\delta_s/l_s$:

$$\frac{\delta_s}{l_s} \sim \tan \theta. \tag{17}$$

Note that this relationship is analogous to one of the key assumptions underlying Chapman's [2] free interaction model, viz, the displacement of the external inviscid flow is determined by the streamwise rate of boundary layer growth. Using (17) in (14) and solving for $\delta_s$ finally yields an estimate for the boundary layer thickness near $x_s$:

$$\delta_s \sim \frac{\mu M_2 a_2 \cos \theta}{(P_p - P_1) \tan \theta}, \tag{18}$$

where $U_2 = M_2 a_2 \cos \theta$ and $a_2$ is the sound speed.

Before proceeding, and as an aside, we rewrite the estimate in (18) as

$$\frac{\mu U_2 / \delta_s}{P_p - P_1} \sim \frac{\tau_2}{\Delta P} \sim \tan \theta. \tag{19}$$

Recognizing that the resultant stress on a fluid particle near $x_s$ is approximately equal to the vector sum of the horizontally acting viscous shear stress, $\tau_2$, and the vertically-acting net pressure, $\Delta P = P_p - P_1$, then (19) shows that the

resultant acts in the direction of the separating boundary layer, $\theta$, as it must. Since $\delta_s/l_s \sim \tan\theta$, then (19) is also consistent with Chapman's [2] estimate for $\tau_2/\Delta P$. Likewise, Chapman et al. [2] argued that $\delta^*/l_s \sim C_f = \tau_w/(\rho_1 u_1^2/2)$, where $C_f$ is the friction factor; since $\tau_w \sim \Delta P$, then for nominally fixed $\theta$ (see Section 2.4 below), (19) is also consistent with Chapman's estimate for $C_f$.

Returning to Eq. (12), inserting (18) and the expression for $R^{-1}$ and rearranging leads to an expression of the following form:

$$\left(\frac{P_p}{P_1}\right)^2 - (1+G)\frac{P_p}{P_1} + G(1+\epsilon) \sim 0, \tag{20}$$

where $G = P_2/P_1$, $\epsilon = kM_2^3 \cos\theta \mu_2 f''/(P_1 f')$, $\mu_2$ is the gas viscosity near the separation point, and where the approximation $\tan\theta \approx -f'$ has been used. Under typical conditions, e.g., those extant in experiments described below [$M_i \approx 5$, $\theta \approx 16°$, $T_o = 310$ K, $P_o = 1.24$ Mpa], $\epsilon = \mathrm{O}(10^3)$, i.e., $\epsilon \ll 1$ [where $f''|_{\max} \approx (\mathrm{d}\theta/\mathrm{d}x)_{\max} = \mathrm{O}(1)$]. Thus, solving (20) for $P_p/P_1$ and neglecting terms smaller than $\mathrm{O}(\epsilon)$, we finally obtain

$$\frac{P_p}{P_1} \sim G - \epsilon\frac{2G}{G-1}. \tag{21}$$

In the following, we will neglect the $\mathrm{O}(\epsilon)$ second term in this equation. Importantly, and in slight contrast with (9), this equation shows that $P_1/P_p \approx P_i/P_p \sim P_1/P_2$, *demonstrating that the separation pressure ratio essentially corresponds to the oblique shock pressure ratio.*

### 2.4. Shock and flow deflection angles

In order to close the approximate models embodied in (9) and (21), it is necessary to specify the shock angle, $\beta$, and the flow deflection angle, $\theta$. Referring to earlier work, Summerfield et al. [23] used measured separation pressure ratios and Mach numbers in the oblique shock relations to infer $\theta$; based on their data, they inferred a nominally fixed value, $\theta \approx 16°$. Using the same approach, Frey [27] likewise found that $\theta$ remained essentially constant for the data sets he analyzed. By contrast, Ostlund [8], again using the same approach, argued that $\theta$ varies with $M_i$, albeit weakly; he fit his estimate with a linear relationship, $\theta = 1.678M_i + 9.347$, valid for $2.5 \leqslant M_i \leqslant 4.5$. For this range of $M_i$, however, the correlation indicates that $\theta$ only varies from $13.5°$ and $16.9°$. Based on these indirect estimates, we assume that $\theta$ is constant; for simplicity, we will arbitrarily adopt the average value of $\theta$ indicated by Ostlund's correlation, $\theta \approx 15.2°$, nearly equal to Summerfield's [23] estimate. Second, we follow Summerfield [23] and assume that the oblique shock relation

$$\tan\theta = \frac{2\cot\beta(M_1^2 \sin^2\beta - 1)}{(k+1)M_1^2 - 2(M_1^2 \sin^2\beta - 1)} \tag{22}$$

applies to the inviscid flow outside the separating boundary layer.

## 3. Auxiliary models

One of the objectives of this work centers on investigating the suitability of simple models for studying and predicting separation in rocket nozzles. Having developed the preceding scaling analyses, we now briefly review Chapman's [2] free interaction model of shock-induced boundary layer separation and review the classical generalized quasi-one-dimensional compressible flow model [31,32], where the latter will be used to investigate flow upstream of separation. As an aside, and with regard to our use of the quasi-one-dimensional model, we note that a variety of other approaches can be used to compute the inviscid upstream flow, including, e.g., MacCormack's method for solving Euler's equations [33] and the method of characteristics. Here, consistent with the approximate nature of the separation models derived, and more importantly, in keeping with our goal of identifying the simplest possible approach, we have chosen the quasi-one-dimensional model.

### 3.1. Free interaction model

Chapman's [2] original analysis posited that thickening of the boundary layer displacement thickness displaced the inviscid flow above the boundary layer according to

$$P(x) - P_i = \frac{\rho_i u_i^2}{\sqrt{M_i^2 - 1}} \, \mathrm{d}\theta, \tag{23}$$

where $\mathrm{d}\delta^*/\mathrm{d}x = \mathrm{d}\theta$, and where the subscripts refer to conditions at $x_i$. He then estimated terms in the balance between the axial pressure gradient and cross-stream shear stress gradient as

$$\frac{P - P_i}{l_s} \sim \frac{\tau_{wi}}{\delta^*} \tag{24}$$

(where $\tau_{wi}$ is the wall shear stress near $x_i$), then estimated $\mathrm{d}\delta^*/\mathrm{d}x$ as $\delta^*/l_s$ (where $\delta^* \sim \delta_s$), and finally combined and linearized (for small $P - P_i$) to obtain

$$\frac{P - P_i}{q_i} \sim \frac{\sqrt{C_{fi}}}{(M_i^2 - 1)^{1/4}}, \tag{25}$$

where $q_i = \rho_i u_i^2/2$ and $C_{fi} = \tau_{wi}/q_i$.

Dividing the left side of (25) by the right suggests that

$$\frac{P - P_i}{q_i} \frac{(M_i^2 - 1)^{1/4}}{\sqrt{C_{fi}}} \sim f(x - x_i) \tag{26}$$

i.e., that the term on the left depends only on position within the shock interaction zone. Erdos and Pallone [13] exploited this idea to develop a wall pressure correlation, $F(s)$, which describes the self-similar pressure variation over the shock interaction zone, where

$$F(s) = \frac{P - P_i}{q_i} \frac{(M_i^2 - 1)^{1/4}}{\sqrt{2C_{fi}}} \tag{27}$$

and where $s = (x - x_i)/(x_s - x_i)$. Carriere et al. [14] extended this work by developing a generalized version of (27), suitable for the non-uniform flows in nozzles. In this case, the self-similar pressure variation over the separation zone is described by

$$F(s; p') = \sqrt{\frac{P - P_i}{q_i} \frac{\bar{\nu}(s) - \nu(s)}{\sqrt{C_{fi}}}}, \tag{28}$$

where $p' = (\delta_i^*/q_i)(\mathrm{d}P/\mathrm{d}x)$ is the normalized inviscid flow pressure gradient immediately upstream of $x_i$, $\nu(s)$ is the Prandtl–Meyer function, and $\bar{\nu}(s)$ is the value of the function in the absence of separation. For a range of pressure gradients observed in a number of different nozzles, the two correlations, $F(s)$ and $F(s; p')$, are nearly identical [8].

Given $F(s; p')$ (or $F(s)$), the predicted separation pressure ratio, $P_i/P_p$, can be determined from either (27) or (28); in the latter case, we follow Chapman [2] and linearize (28) to obtain

$$\frac{P_i}{P_p} = \left[ F(s_p; p')kM_i^2 \frac{\sqrt{C_{fi}}}{\sqrt{2}\,(M_i^2 - 1)^{1/4}} + 1 \right]^{-1}, \tag{29}$$

where $\bar{\nu}(s)$ is approximated as $\nu_i$ and where $F(s_p; p')$ [$= 6.0$; see [8]] is the value of $F(s; p')$ at the effective separation point, $s_p$ [$= (x_p - x_i)/(x_s - x_i)$]. It is important to note that Ostlund [8] has developed an alternative separation criterion which requires a priori specification of both the plateau pressure, $P_p$, and the friction coefficient, $C_{fi}$ at $x_i$. The criterion in (29) by contrast only requires information on $C_{fi}$. Fortuitously, and as originally shown by Chapman et al. [2], for shock-induced separation of *turbulent* boundary layers, the dependence of $P_i/P_p$ on $C_{fi}$ (or equivalently, on $Re_{\delta^*}$, the displacement thickness Reynolds number at $x_i$) is weak, at least over the range of Mach numbers investigated ($1.3 \leqslant M_i \leqslant 4.0$), consistent with both the second scale analysis above and previously developed correlations [8,19,24–27].
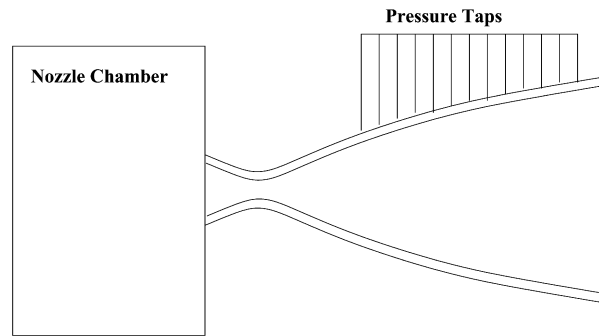
Fig. 3. Schematic of Nozzle Test Facility. Throat diameter is 2.54 cm, ratio of nozzle exit to throat areas is 30:1, nozzle length (from chamber) is 67.8 cm, and tap spacing is 2.54 cm.

### 3.2. Generalized quasi-one-dimensional flow model

Full descriptions of this model are presented, for example, by Shapiro [31] and Oosthuizen and Carscallen [32]. Here, we describe only the results relevant to the present study. The variation of free stream Mach number within a variable area, adiabatic duct subject to friction at the wall is given by

$$\frac{\mathrm{d}M^2}{M^2} = \frac{1 + (k-1)M^2/2}{1 - M^2}\left[-2\frac{\mathrm{d}A}{A} + kM^2 f \frac{P}{A}\,\mathrm{d}x\right], \tag{30}$$

where $A$ is the local cross-sectional area, $P$ is the corresponding perimeter, and $f = C_f$ is the Fanning friction factor. Based on measurements described in Section 4 below, this simple model appears to provide a reasonably accurate description of nozzle wall pressure variations upstream of separation.

## 4. Experimental measurements

A series of experiments were carried out in the Nozzle Test Facility at Marshall Space Flight Center. The experiments were designed to investigate the role of boundary layer separation on nozzle side-loading and to examine fluid–solid interactions underlying oscillatory modes observed in side-loaded nozzles.

A sub-scale, ideal-contour nozzle, having an area ratio of approximately 30:1 (exit to throat area) was operated under a range of cold-flow, overexpanded conditions. The nozzle was outfitted with a series of pressure taps, as shown schematically in Fig. 3, where tap spacing in the axial direction was 0.0254 m. Two sets of azimuthally spaced taps were also used, placed at two axial locations, at 45° intervals around the nozzle circumference. The axially-spaced taps allow measurement of the instantaneous and time-average axial pressure distribution within the nozzle while the azimuthally distributed taps allow examination of the instantaneous and time-average separation line (under conditions where the shock interaction zone coincides with either set of azimuthally distributed taps).

The experimental nozzle was, on one hand, designed to approximately emulate the MC-1 nozzle [34], while on the other, maximize anticipated separation loading. Given the non-standard nature of the design, we list in Table 1 information on nozzle radius as a function of axial position; see Appendix A. The throat diameter was 0.0254 m and the design Mach number was 5.25.

Pressures at all taps were sampled at 10 kHz, sufficiently high to allow study of the low-frequency, large-amplitude component of shock motion [4], but not sufficient to resolve small-scale, high frequency jitter. Once nominally steady conditions were achieved, pressure data was taken from all taps for a period of 8.3 seconds. Finally, dehumidified air was used in all tests, eliminating the potential for condensation shock formation.

## 5. Results and discussion

### 5.1. Model I and II separation pressure ratios

The scaling relationships in (9) and (21) were fit to available data on separation in overexpanded nozzles. Data on free shock separation was obtained from a number of sources [15,19,20,35,36], and represents flow in a variety of
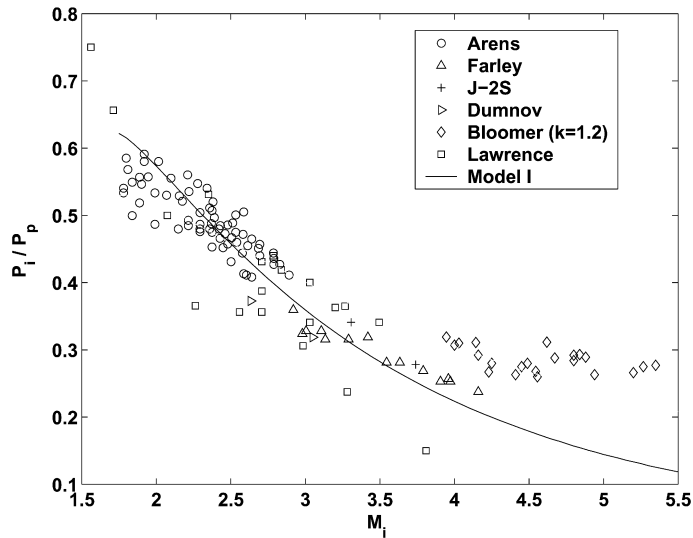
Fig. 4. Comparison of model I with separation measurements in rocket engine nozzles. The fitting constant equals 1.52.
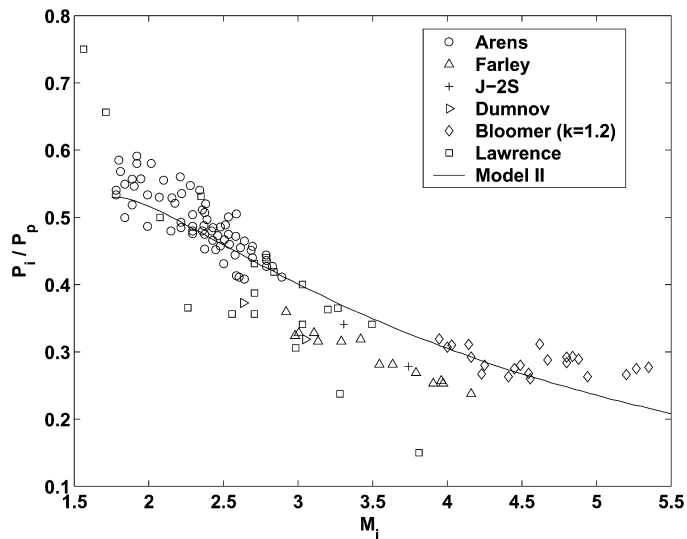


Fig. 5. Comparison of model II with separation measurements in rocket engine nozzles. The fitting constant equals 1.14.

nozzle geometries, in both full-scale and sub-scale models, under both cold flow and hot fire conditions. Although the working fluid in most experiments was air, Bloomer's [20] hot fire measurements, which used a mixture of JP-4 rocket fuel and liquid oxygen ($k = 1.2$), are included in estimating best fit parameters. This approach is allowable due to the weak dependence between separation pressure ratio and $k$ [16,19]. Since solutions for $P_1/P_2$ at a turning angle of $\theta = 15.2°$ do not exist for $M_i \lesssim 1.7$ [19], only data obtained at $M_i \geqslant 1.75$ are used in the fitting procedure. For comparative purposes, however, the limited data available at $M_i \leqslant 1.75$ are presented in the graphs below.

A comparison of separation pressure ratios predicted by model I [Eq. (9)] with available data, shown in Fig. 4, indicates that the model provides reasonable predictions over the range $1.75 \leqslant M_i \leqslant 4.0$. The least square fitting constant is found to be 1.52. A similar comparison using model II, shown in Fig. 5, likewise indicates reasonable agreement over $1.75 \leqslant M_i \leqslant 4.5$, with significantly improved agreement for $M_i > 4.0$; the fitting constant in this case is 1.14. Comparing with Ostlund [8] and Frey's [27] ad hoc correlations, which fit observed shock pressure ratios to the oblique shock pressure ratio (based on inferred shock and deflection angles), we note that their quoted ranges of validity were in both cases $2.5 \leqslant M_i \leqslant 4.5$.
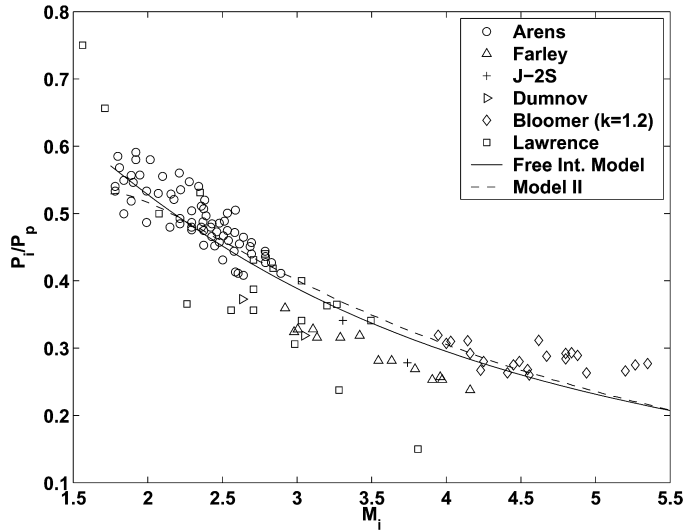
Fig. 6. Comparison of free interaction model and model II with separation measurements in rocket engine nozzles.

At higher Mach numbers ($M_i \geqslant 4$), the data suggests that $P_i/P_p$ becomes largely independent of $M_i$. Although constancy of $P_i/P_p$ is not inconsistent with separation remaining dominated by the oblique shock, since the asymptotic expressions for $P_i/P_p$ at large $M_i$ are, from (9) and (21),

$$\frac{P_i}{P_p} \sim \frac{\sin^2(\beta - \theta)}{\sin^2 \beta M_i^2}$$

and

$$\frac{P_i}{P_p} \sim \frac{k+1}{2k \sin^2 \beta M_i^2}$$

respectively, then due to an 82% variation in $M_i^2$ over $4.0 \leqslant M_i \leqslant 5.4$, the time-average deflection angle, $\theta$, likely becomes moderately dependent on $M_i$.

### 5.2. Separation pressure ratios via the free interaction model

In order to use the free interaction separation criterion in (29), $C_{fi}$ must be specified. As noted, and based on Chapman's [2] observation that $P_i/P_p$ is weakly dependent on $C_{fi}$, we assume that $C_{fi}$ is constant. The assumed magnitude, $C_{fi} = 0.00245$, represents the characteristic value obtained from fitting the free interaction model to observed time-average shock interaction zone pressure variations, as described in Section 5.4.2 below. In addition, this value is used in fitting the generalized quasi-one-dimensional flow model to our experimental shock-free flow measurements, as described in Section 5.4 below.

As shown in Fig. 6, over $1.75 \leqslant M_i \leqslant 5.5$, predicted separation pressure ratios obtained via the free interaction model are quite similar to those obtained via the second scaling analysis above. Given the reasonable agreement between model predictions and previous observations, this result simplifies Ostlund's [8] separation criterion by eliminating the need for *a priori* specification of $P_p$. Importantly, this result provides further evidence of the applicability of the free interaction model to separation in nozzles, and moreover, further indicates the physical consistency of the second scale analysis above.

### 5.3. Model I and II reconsidered

Having obtained further evidence that separation in overexpanded nozzles is a free interaction problem, we are confronted with two important questions. First, which approximate model, I or II, provides a more realistic rendering of shock-induced turbulent boundary layer separation in nozzles? Second, and more broadly, does either model apply
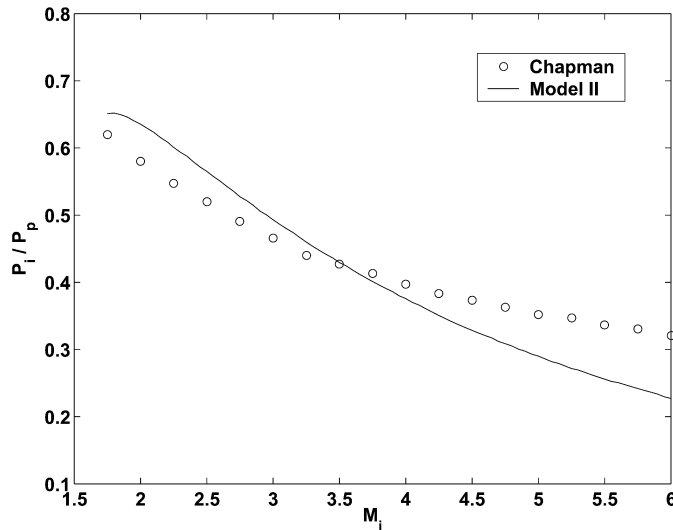
Fig. 7. Comparison of model II with separation measurements for flow over backward facing steps (Chapman et al. [2]). The fitting constant equals 1.40.

to the family of free interaction problems encompassed by the free interaction theory? Three observations suggest that model II provides both an accurate description of separation in nozzles, and a realistic description of separation in free interaction problems. First, as shown in Fig. 7, it is found that model II provides reasonable predictions of Chapman's [2] separation pressure data for supersonic flow over backward facing steps (where we follow Chapman and assume a constant flow deflection angle of $16°$ and where the fitting constant is 1.41). Model I by contrast, is not predictive in this case (result not shown). Second, as shown above (Fig. 6), predicted separation pressure ratios obtained via model II are nearly identical to those obtained via the free interaction model. Third, the qualitative and quantitative validity of the scaling argument underlying model II is strongly indicated by the fact that the fitting constant is close to 1 (1.14).

### 5.4. Results and analysis of present separation measurements

Although the spatial resolution of our pressure measurements is fairly course, normalized time average axial pressure distributions, $P/P_o$, within the nozzle are found to exhibit the classical features of free shock separation (as shown schematically in Fig. 1): near-isentropic pressure decay from the throat to the nominal incipient separation point, $x_i$, rapid pressure rise from $Xi$ through the nominal separation point, $x_s$ (where the latter can be determined, for example, using surface tracer methods [37], and leveling off to a plateau pressure, $P_p$, in the vicinity of the shock-interaction zone's lower-most reach, $x_p$ (results not shown).

Considering flow upstream of incipient separation, it is found that the variation in wall pressure, $P/P_o$, can be predicted with reasonable accuracy using the generalized quasi-one-dimensional model described in Section 3.2 above; see Fig. 8. The plot shown is obtained for shock-free flow conditions using a least squares fitting procedure in which the sonic point, $x_o$, and Mach number, $M_0$, immediately downstream of $x_o$ serve as fitting parameters; as before, the friction factor, $C_f$, is assumed constant and equal to 0.00245. Although the theoretical sonic point can be determined using the generalized quasi-one-dimensional flow model [32], due to indeterminate frictional losses and heat transfer between the nozzle chamber and throat, the theoretical expression (incorporating only estimated frictional and area change effects) leads to unacceptable results. The fitting procedure leads to an estimated sonic point 1.5 cm downstream of the throat ($x/r_t = 0.59$) and an initial Mach number of 1.035 (at a position 0.1 cm downstream of the sonic point).

#### 5.4.1. Separation locations via the generalized quasi-one-dimensional model

Importantly, we find that the generalized quasi-one-dimensional flow model can be used to predict the nominal separation locations observed in our experiments. Prior to discussing this result, we note that due to the spatial courseness
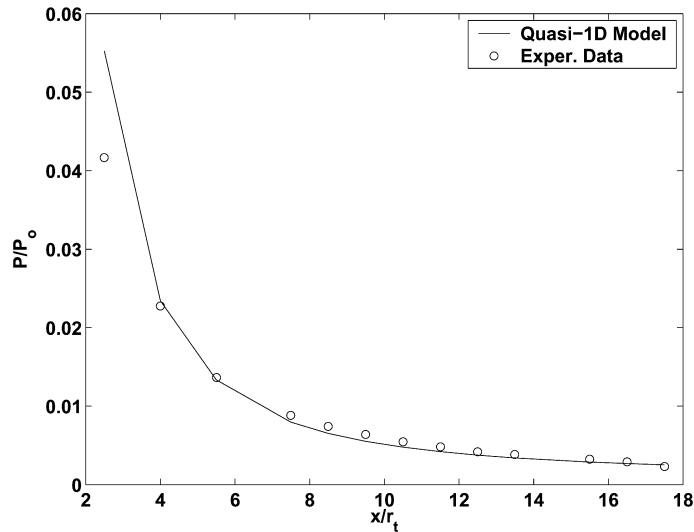
Fig. 8. Comparison of generalized quasi-one-dimensional flow model with observed time-average, shock-free wall pressure variation. Estimated sonic point 1.5 cm downstream of the throat; estimated initial Mach number (immediately downstream of sonic point) is 1.035; the assumed friction coefficient is 0.00245; $r_t$ = nozzle radius.

of our pressure measurements, and as an alternative to determining $P_i/P_p$ versus $M_i$, we plot the most-downstream measurement location at which the boundary layer remains attached to the wall as a function of the nozzle pressure ratio, NPR ($= P_o/P_a$, where $P_o$ is the nozzle chamber pressure); the former is determined using methods outlined in Dolling and Brusniak [4]. This approach is taken since it provides a unambiguous indication of the uncertainty associated with typical separation pressure estimates, i.e., those based on spatially course pressure measurements, while allowing an assessment of the potential utility of the quasi-one-dimensional model in predicting separation line locations. Indeed, as a means of reducing the uncertainty that characterizes existing separation pressure estimates, we would argue that future estimates should only incorporate high resolution pressure measurements.

Due to the uncertainty associated with our (spatially course) pressure measurements, we have not included our $M_i$ and $P_i/P_p$ data in the plots shown in Figs. 4–6. We note, however, that over the limited range of separation Mach numbers extant in our experiments, $5.0 \leqslant M_i \leqslant 5.4$, estimated separation pressure ratios, $P_i/P_p$, are essentially constant and equal to 0.3, consistent with Bloomer's [20] earlier observations. [In the present study, $P_i/P_p$ is estimated as the ratio of the pressure at the *detected* incipient separation point, $x_i$, i.e, the measurement location where wall pressure begins to rise, to the observed plateau pressure.]

In order to use the generalized quasi-one-dimensional model to predict separation locations, we first express $P_i/P_p$ as

$$\frac{P_i}{P_p} = \frac{P_i}{P_o}\frac{P_o}{P_p} \approx \frac{P_i}{P_o}\frac{P_o}{P_a} = \frac{P_i}{P_o}NPR,$$

where the peak pressure, $P_p$, is approximated as the ambient pressure, $P_a$ [8,16,27]. In reality, a small static pressure rise from $P_p$ to $P_a$ is typically observed, likely reflecting inward acceleration of ambient gas through the recirculation zone toward the separation point [as depicted, e.g., in Fig. 2]. Since stagnation pressure, $P_o$ ($= P + \rho u^2$), within the recirculation zone remains essentially fixed while dynamic pressure, $\rho u^2$, increases due to inward acceleration, the static pressure, $P$, as detected at the nozzle wall, must decrease from the exit toward the separation point [38].

Next, we express $P_i/P_o$ as $P_i/P_o = G(M_i)$, where $G(M_i)$ is the value of $P_i/P_o$ predicted by the generalized quasi-one-dimensional model at $M_i$. The ratio $P_i/P_p$ is then expressed as $P_i/P_p = F_o(M_i)$, where again $F_o(M_i)$ is the separation pressure ratio predicted by a given separation criterion, e.g., (9), (21), or (29). Combining, we finally obtain an expression relating the separation Mach number to the nozzle pressure ratio:

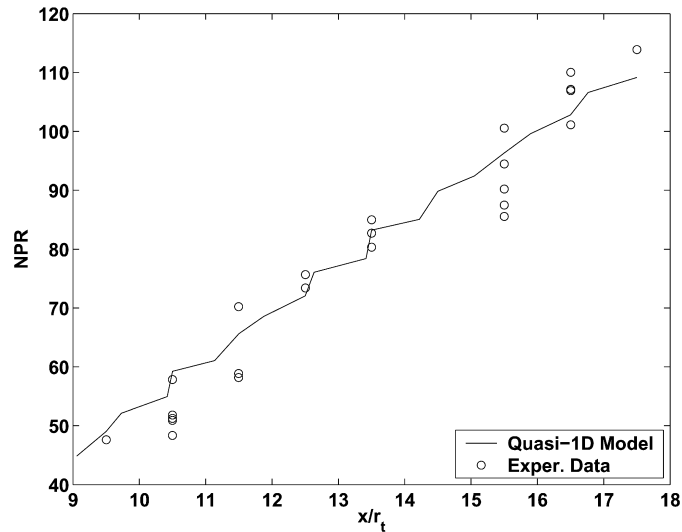$$NPR = \frac{F_o(M_i)}{G(M_i)}. \tag{31}$$

Fig. 9. Comparison of separation locations predicted by the generalized quasi-one-dimensional flow model with experimental observations.

Thus, for a given NPR, $M_i$ can be determined from (31) and then used to determine the separation location (e.g., via the quasi-one-dimensional model).

Here, since the range of separation Mach numbers extant in our experiments, $5.0 \leqslant M_i \leqslant 5.4$, lies beyond the range of validity of models I and II, and beyond that of the free interaction criterion in (29), we assume a constant separation pressure ratio, $P_i/P_p = F_o(M_i) = 0.285$; this represents the average of Bloomer's [20] estimated separation pressure ratios, indicated in Figs. 4–6, and our estimates described immediately above. The results, shown in Fig. 9, demonstrate that approximate separation locations can be predicted with reasonable accuracy over a wide range of nozzle pressure ratios. Note that the uneven appearance of the theoretical plot reflects the use of unevenly spaced, spatially coarse nozzle geometric data in the integration used to compute $G(M_i)$. Note too that the sonic point, $x_o$ ($= 0.015$ m downstream of the throat), initial Mach number, $M_o$ ($= 1.035$), and friction coefficient, $C_f$ ($= 0.00245$) determined above are used in the calculations.

A rough estimate of actual time-average separation locations can be obtained as follows: when the maximum NPR for which the boundary layer remains attached at a given measurement location, $x_{m,i}$, is approximately equal to the minimum NPR (for attached flow) at the adjacent downstream measurement location, $x_{m,i+1}$, the actual separation point can be assumed to lie near $x_{m,i+1}$. Thus, based on this rough criterion, it is seen that predicted separation line locations generally lie near or somewhat upstream of actual. Although not shown, it is found that predictions are sensitive to $M_o$, but are relatively insensitive to $C_f$: a 1% variation in $M_o$ leads to approximate 10% variations in predicted NPR's while over the range $0.002 \leqslant C_f \leqslant 0.004$, predicted NPR's (at any given location) vary by less than 15%. Thus, in application, a reliable method for estimating or measuring $M_o$ is required. From a practical standpoint, this result suggests that as a preliminary design tool, the generalized quasi-one-dimensional model may provide sufficient accuracy when assessing separation locations in nozzles. Computationally, the model may likewise provide a simple alternative or adjunct to complex simulations.

### 5.4.2. Free interaction model comparison

Observed time-average pressure variations over the shock interaction zone were compared against those predicted by the free interaction model, with a representative result shown in Fig. 10. The comparison is representative of the range of nozzle pressure ratios for which a well-defined plateau pressure could be determined, $47 \leqslant NPR \leqslant 100$ [where $NPR = 47$ is the lowest ratio tested].

The model was fit to the data by treating the length $l_s = x_s - x_i$, and the friction coefficient, $C_{fi}$ at $x_i$ as fitting parameters. This contrasts with the approach taken by Ostlund [8] who computed $C_{fi}$ and used $x_i$ and $l_s$ as fitting parameters. In reality and as mentioned, the free interaction model incorporates anywhere from one to four parameters, $x_i$, $l_s$, $C_{fi}$, and $p'$, any subset of which can be estimated, depending on the amount of experimental information available. Here, in order to obtain reasonable estimates of $x_i$, we focused on those experiments (described immediately
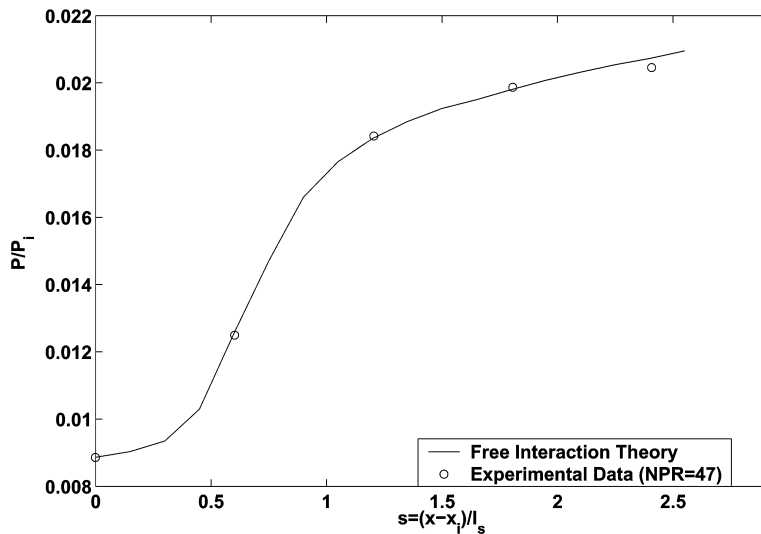
Fig. 10. Comparison of shock interaction zone pressure variation predicted by free interaction model with data ($NPR = 47$). Here, estimated values for $l_s$ and $C_{fi}$ are 0.021 m, and 0.00223, respectively.

above) in which the maximum NPR for attached flow at a given measurement location was approximately equal to the minimum NPR for attached flow at the adjacent downstream measurement site; as noted, this allows one to identify the downstream measurement site as the approximate separation location. Although this approach is subject to uncertainty, it was found that corresponding fits were reasonably accurate, as indicated in Fig. 10. By contrast, due to the spatial coarseness of our measurements (and corresponding paucity of data over the shock interaction zone), fits in which $l_s$ and $x_i$, or $C_{fi}$, $x_i$, and $l_s$ served as fitting parameters were generally poor. Strictly speaking, and with regard to the present results and those in Ostlund [8], a rigorous test of the free interaction model's ability to capture the structure of the shock interaction zone will require use of well-established model parameters.

## 6. Summary and conclusions

Time-average, shock-induced, turbulent boundary layer separation has been investigated using a combination of heuristics, simple analytical models, and experiments, with a focus on separation in overexpanded rocket nozzles. Two simple scaling analyses are presented in which separation is viewed as reflecting a balance between streamwise boundary layer inertia and the cross-layer pressure gradient. These lead to two theoretical expressions for the time-average separation pressure ratio, stated as a function of the inviscid Mach number at the point of incipient separation. In both models, explicit relationships between the separation pressure ratio (at the wall) and the classical oblique shock ratio are obtained; the second model, representing a refinement of the first, demonstrates for the first time that the separation pressure ratio is, to a good approximation, determined by the oblique shock pressure ratio.

Comparisons with available data suggest that the second model provides a fairly realistic picture of time-average separation in overexpanded nozzles, and more generally, of separation in free interaction problems. In addition, an examination of Chapman's [2] free interaction theory shows that nozzle separation pressure ratios predicted by this model are quite similar to those obtained by the second scale analysis.

Experimentally observed time-average wall pressure distributions upstream of separation can be predicted with reasonable accuracy using the classical generalized quasi-one-dimensional flow model. Significantly, the model can be used in combination with suitable boundary layer separation criteria to estimate time-average separation locations. In addition, preliminary results indicate that the free interaction model is capable of providing accurate descriptions of the time-average pressure variation over the shock interaction zone, in agreement with Ostlund's [8] recent findings.

Finally, we note that due to the sensitivity of the separation process to a number of typically coupled features, e.g., nozzle shape, gas temperature, interior shock structure, and external conditions, a fair degree of uncertainty will likely remain associated with separation prediction. However, efforts could be undertaken to both improve repeatability of experimental measurements and physical understanding of separation. First, as noted in Section 5.4, separation data,

i.e., wall pressure measurements, can be significantly improved by increasing the spatial resolution of separation zone measurements. Second, improved models of separation zone flow physics are required. While earlier studies, e.g., [2,13,14], along with the present investigation, provide some framework for understanding free shock separation, work is needed, for example, to understand shock/shock foot interactions with boundary layer vortical structures, dynamic interactions between the separated boundary layer and separation-inducing shock, and on the potential importance of upstream information propagation (of downstream conditions) within the subsonic (very-near-wall) portion of the incipiently separating boundary layer.

## Acknowledgements

## Appendix A

Table 1
Experimental nozzle geometry (all dimensions in cm)

| Axial position | Nozzle radius | Axial position | Nozzle radius |
| --- | --- | --- | --- |
| 0.00000 | 3.96240 | 9.98220 | 2.69494 |
| 1.87960 | 3.96240 | 10.03300 | 2.71780 |
| 3.45440 | 3.94462 | 10.31240 | 2.83210 |
| 7.51840 | 2.70002 | 11.2776 | 3.26898 |
| 7.64540 | 2.65684 | 12.6492 | 3.90652 |
| 9.09320 | 2.54000 | 14.3510 | 4.66852 |
| 9.19480 | 2.54254 | 16.2814 | 5.49402 |
| 9.29640 | 2.54762 | 18.4658 | 6.35254 |
| 9.37260 | 2.55524 | 20.8788 | 7.22122 |
| 9.44880 | 2.56286 | 23.5204 | 8.08482 |
| 9.49960 | 2.57302 | 26.4160 | 8.93572 |
| 9.57580 | 2.58572 | 29.5402 | 9.76630 |
| 9.65200 | 2.60096 | 32.8930 | 10.56894 |
| 9.70280 | 2.61366 | 36.4490 | 11.3411 |
| 9.75360 | 2.62128 | 40.2590 | 12.0777 |
| 9.80440 | 2.63652 | 44.2976 | 12.7787 |
| 9.85520 | 2.65176 | 48.5648 | 13.4366 |
| 9.90600 | 2.66700 | 53.0352 | 14.0513 |
| 9.95680 | 2.68224 | 55.3466 | 14.3434 |

## References

[1] G. Settles, Details of a shock-separated turbulent boundary layer at a compression corner, AIAA J. 14 (1976) 1709.

[2] D.R. Chapman, D.M. Kuehn, H.K. Larson, Investigation of separated flows in supersonic and subsonic streams with emphasis on the effect of transition, NACA Report 1356, 1958.

[3] M.E. Erengil, D.S. Dolling, Correlation of separation shock motion with pressure fluctuations in the incoming boundary layer, AIAA J. 29 (1990) 1868.

[4] D.S. Dolling, L. Brusniak, Separation shock motion in fin, cylinder, and compression ramp-induced turbulent interactions, AIAA J. 27 (1988) 734.

[5] J. Ackeret, F. Feldman, N. Rott, Investigations of compression shocks and boundary layers in gases moving at high speed, NACA TM 1113, 1947.

[6] D.S. Dolling, D.R. Smith, Separation shock dynamics in Mach 5 turbulent interactions induced by cylinders, AIAA J. 27 (1989) 1698.

[7] R.A. Gramann, D.S. Dolling, Detection of turbulent boundary-layer separation using fluctuating wall pressure signals, AIAA J. 28 (1989) 1052.

[8] J. Ostlund, Flow processes in rocket engine nozzles with focus on flow-separation and side-loads, Licentiate Thesis, Royal Inst. of Tech., Stockholm, TRITA-MEK, Tech. Rept. 2002:09, 2002.

[9] D.D. Knight, G. Degrez, Shock wave boundary layer interactions in high Mach number flows: a critical survey of current numerical prediction capabilities, AGARD Advisor Rep. 319, vol. II, 1998.

[10] G.E. Gadd, D.W. Holder, J.D. Regan, An experimental investigation of the interaction between shock waves and boundary layers, Proc. Roy. Soc. London Ser. A 226 (1954) 227.

[11] S.M. Bogdonoff, Some experimental studies of the separation of supersonic turbulent boundary layers, Rept. 336, Aeronautical Engineering Dept., Princeton Univ., 1955.

[12] H.W. Liepmann, A. Roshko, S. Dhawan, On reflection of shock waves from boundary layers, NACA Report 1100, 1952.

[13] J. Erdos, A. Pallone, Shock-boundary layer interaction and flow separation, in: Proc. Heat Transfer and Fluid Mechanics Inst., Stanford Univ. Press, 1962.

[14] P. Carriere, M. Sirieix, J.L. Solignac, Properties de similitude des phenomenes de decollement laminaires ou turbulents en ecoulement supersonic nonuniforme, in: 12th Int. Congress of Appl. Mech., Stanford Univ., 1968.

[15] G.E. Dumnov, Unsteady side-loads acting on the nozzle with developed separation zone, AIAA Paper 96-3220, 1996.

[16] M. Frey, G. Hagemann, Status of flow separation prediction in rocket nozzles, AIAA Paper 98-3619, 1998.

[17] C.R. Foster, F.B. Cowles, Experimental study of gas flow separation in overexpanded nozzles for rocket engines, Calif. Inst. Tech. Progr. Rept. 4-103, 1949.

[18] J.D. McKenney, Ae.E. Thesis, Calif. Inst. Tech., 1949.

[19] M. Arens, E. Spiegler, Shock-induced boundary layer separation in overexpanded conical exhaust nozzles, AIAA J. 1 (1963) 578.

[20] H.E. Bloomer, R.J. Antl, P.E. Renas, Experimental study of the effects of geometric variables on performance of conical rocket engine exhaust nozzles, NASA TN D-846, 1961.

[21] S. Deck, P. Guillen, Numerical simulation of side loads in an ideal truncated nozzle, J. Propulsion and Power 18 (2002) 261.

[22] L.H. Nave, G.A. Coffey, Sea-level side-loads in high area ratio rocket engines, AIAA Paper 73-1284, 1973.

[23] M. Summerfield, C.R. Foster, W.C. Swan, Flow separation in overexpanded supersonic exhaust nozzles, Jet Propulsion 24 (1954) 319.

[24] T.W. Schilling, Flow separation in rocket nozzle, M.S. Thesis, Univ. of Buffalo, 1962.

[25] S. Kalt, D. Badal, Conical rocket nozzle performance under flow separated condition, J. Spacecraft Rockets 2 (1965).

[26] R. Schmucker, Flow processes in overexpanded nozzles of chemical rocket engines, Rept. TB-7, -10, -14, Technical Univ. of Munich, 1973.

[27] M. Frey, Behandlung von Stomungsproblemen in Rakendusen bei Überexpansion, Ph.D. Dissertation, Institut für Aerodynamic and Gasdynamic Universität Stuttgart, 2001.

[28] L. Crocco, R. Probstein, The peak pressure rise across an oblique shock emerging from a turbulent boundary layer over a plane surface, Princeton Univ., Aero. Engrg. Dept., Kept. 254, 1954.

[29] J. Delery, J.G. Marvin, Shock-wave boundary layer interactions, AGARD No. 280, 1986.

[30] S.M. Bogdonoff, C.E. Kepler, Separation of a supersonic turbulent boundary layer, Rep. 249, Princeton Univ., Dept. Aero. Engr., 1954.

[31] A.H. Shapiro, The Dynamics and Thermodynamics of Compressible Fluid Flow, Wiley, New York, 1953.

[32] P.H. Oosthuizen, W.E. Carscallen, Compressible Fluid Flow, McGraw-Hill, New York, 1997.

[33] J.D. Anderson, Computational Fluid Dynamics, McGraw-Hill, New York, 1995.

[34] D. Davis, Thermal analysis of the MC-1 chamber/nozzle, in: AIP Conf. Proc., vol. 552, 2001, p. 292.

[35] J.M. Farley, C.E. Campbell, Performance of several methods of characteristic exhaust nozzles, NASA TN D-293, 1960.

[36] R.A. Lawrence, Symmetrical and unsymmetrical separation in supersonic nozzles, Research Rept. 67-1, Southern Methodist Univ., 1967.

[37] G. Settles, T. Fitzpatrick, S. Bogdonoff, Detailed study of attached and separated compression corner flowfields in high Reynolds number supersonic flow, AIAA J. 17 (1979) 579.

[38] C. Hagemann, M. Terhardt, M. Frey, P. Reijasse, M. Onofri, F. Nasuti, J. Ostlund, Flow separation and side-loading in rocket nozzles, in: Proc. 4th Int. Symp. on Liquid Space Propulsion, German Aerospace Center, Lampoldshausen, 2000.